DYNAMIC COMPRESSIBILITY OF POROUS NaCl AT LOW PRESSURES

I. V. Belinskii and B. D. Khristoforov

The dynamic compressibility of porous NaCl of initial density $\rho_{00} = 1.87 - 1.9$ g/cm^3 has been investigated on the pressure interval from 1 to 200 kbar. The dynamic compression parameters are determined from the data of electromagnetic and capacitive measurements of the wave and particle velocities of waves excited by explosion and impact. The results are compared with those of ultrasonic and static measurements. The experimental data indicate the inapplicability of the hydrodynamic model for describing the behavior of porous NaCl under dynamic loading in the region of stresses comparable with its strength.

1. Previous experiments [1, 2] show that at pressures below 100 kbar the parameters of shock waves in solids depend importantly on porosity (or jointing in rocks). At densities of the shock-compressed material close to the crystal density, the wave front is diffused. The entry velocity is close to the velocity of the longitudinal acoustic waves, while the maximum velocity is considerebly lower than the hydrodynamic speed of sound. Features of the behavior of the material associated with elastoplastic effects and the process of pore collapse have an important influence on the dynamic compressibility. So far there has been no reliable description of the behavior of a material in the region of pressures comparable with its strength.

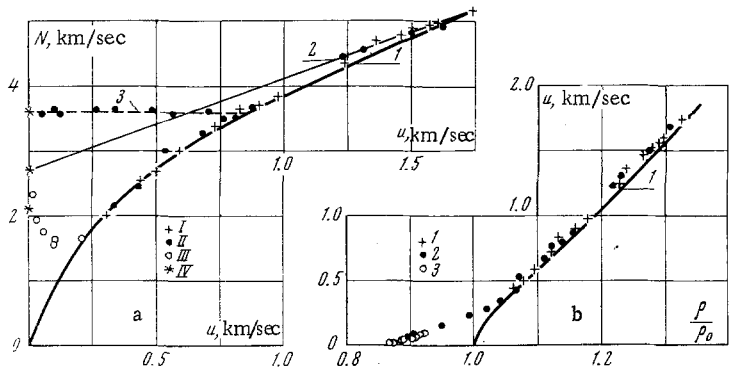

Fig. 1. a) Wave velocity N as a function of the maximum particle velocity u; b) maximum particle velocity u as a function of relative density ρ/ρ_0. 1) Calculation based on Eqs. (1); 2) linear N(u) relation; 3) entry velocity of elastic wave. I) Data of wave and particle velocity measurements; II) data of particle velocity and density measurements, III) impact experiments; IV) ultrasonic measurements.

Moscow. Translated from Zhurnal Prikladnoi Mekhaniki i Tekhnicheskoi Fiziki, Vol. 11, No. 2, pp. 134–139, March-April, 1970. Original article submitted May 15, 1969.

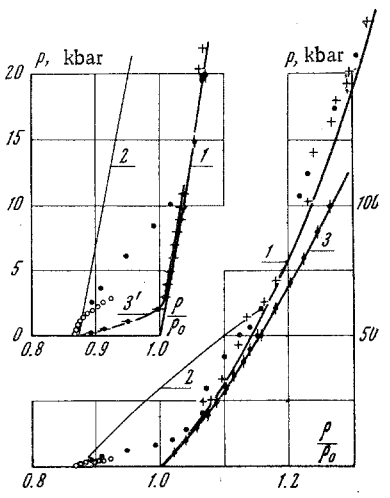

Fig. 2. Normal compressive stress p as a function of the relative density ρ/ρ_0; 1) calculations based on Eqs. (1); 2) Hooke's law for plane strain; 3) Bridgeman's data; 3') static compression data for a NaCl sample with $\rho_{00} = 1.87$ g cm^3 in a rigid ring. At top left the low-pressure region is shown to an enlarged scale.

The shock-compressibility parameters of a porous material calculated from Eqs. (1) by the method of [3, 9] without allowance for its strength are equal to zero at $V = V_0$ (curves 1 in Figs. 1 and 2).

$$p(V, V_{00}) = p_1(V)\frac{V_0 - V - 2V_0/\gamma_0}{V_{00} - V - 2V_0/\gamma_0}$$
$$u = [p(V_{00} - V)]^{1/2},\quad N = V_{00}[p/(V_{00} - V)]^{1/2} \qquad (1)$$
$$V_{00}/V = N/(N - U),\quad \gamma/V = \gamma_0/V_0 .$$

Here, P is the pressure or normal stress of shock compression; u, N are the particle and wave velocities; V_{00} is the initial specific volume of the powder; V_0, γ_0, p_1 are the corresponding crystal parameters. In deriving (1), it is assumed that the initial energies of the solid and porous materials are the same. The approximation for the Gruneisen constant γ is convenient and does not lead to significant errors in the low-pressure region. The $p_1(V)$ relation is taken from [5].

Actually, the process of pore collapse is associated with the destruction and plastic deformation of the powder grains, therefore, at stresses close to the grain strength, the effect is not described by calculations based on the hydrodynamic model. Accordingly, the dynamic compressibility of NaCl powder in the low-pressure region was determined experimentally.

2. Plane shock waves were excited in NaCl samples by explosions or the impact of thin aluminum plates. In the first case, we employed charges of various density 100 and 84 mm in diameter, consisting of a 50/50 TNT/RDX or 50/50 TNT/benzoic acid mixture. The charge and the sample were separated by intervening layers of brass, benzoic acid, or air in order to obtain a shock wave of the necessary intensity with an approximately stepped profile. The use of explosive lenses made it possible to obtain shock waves with a front deviating from the plane by not more than 0.1 μsec on a diameter of 80 mm. The aluminum plates, about 0.5 mm thick, were shot off a brass shield 5 mm thick, in which a plane shock wave was excited by impact. The distortion of these plates did not exceed 0.2 μsec on a diameter of 80 mm. Their velocity was 1.65-1.72 km/sec. We used cylindrical samples of NaCl powder, grain size about 0.3 mm, diameter 84 mm, thickness 2-25 mm, pressed to a density of 1.87 g/cm^3 in the impact experiments and to a density 1.88-1.80 g/cm^3 in the explosion experiments.

In the explosion experiments the particle and wave velocities were measured by the electromagnetic method, using two sensors inserted in the sample a distance 5-7 mm apart. By integrating the particle velocity oscillograms with respect to time, we determined the displacement of the sensor and the density of the material compressed by the shock wave. The signals from the sensors were recorded by two OK-17 oscillographs and at the same time by a single OK-33. The accuracy of the individual measurements of u and N was approximately ± 3%. A systematic error ≈ 3% is possible in measuring the particle velocity. This leads to a lower value, owing to the failure of the measuring channel to allow for the steep drop of the wave front and the internal resistance of the sensor. In the case of impact excitation, we measured the particle velocity by the electromagnetic method at u > 100 m/sec, the free surface velocity w by a capacitive method and the wave propagation time. The moment of impact was registered by a contact sensor. It was assumed that w = 2u over the entire measurement interval. At u > 100 m/sec, both methods of determining the particle velocity gave the same results. In these experiments the wave velocity was determined by graphic differentiation of the entry and wave maximum hodograph constructed from the measured time taken by the wave to travel from the impact surface to the sensor.

In order to determine the elastic characteristics of the samples under normal conditions, we measured the velocities C_1 and C_2 of the longitudinal and transverse acoustic waves by means of a UZIS LETI-4 ultrasonic instrument at a frequency of 1.67 mHz. The measurements were based on a comparsion of the wave propagation times in the sample and a standard consisting of a 18% solution of alcohol in distilled water, in which the speed of sound is 1600 ± 10 m/sec. We used samples with densities from 1.56 to 2.15 g/cm^3 and grain sizes less than 0.11 mm, about 0.3 mm and greater than 0.4 mm, as well as a sample of single-crystal NaCl. The accuracy of the individual ultrasonic measurements was about 3%.

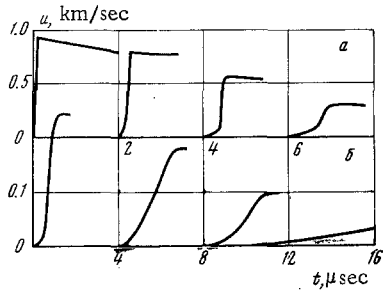

Fig. 3

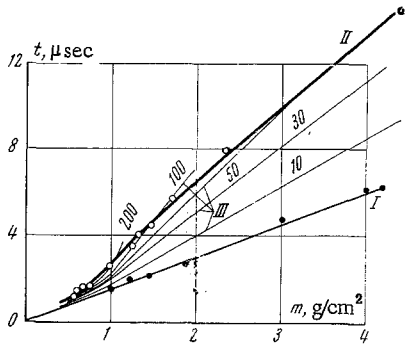

Fig. 4

Fig. 3. Profiles of the particle velocity u as a function of t: a) for explosion; b) for impact.

Fig. 4. m,t-diagram for impact compression: I) wave front; II) unloading wave; III) constant-velocity curves. The figure on curves III correspond to values of the particle velocity u in m/sec.

3. From the measured values of the longitudinal C_1 and transverse C_2 sound velocities we calculated the hydrodynamic speed of sound $C_3 = (K/\rho_{00})^{1/2}$, Poisson's ratio ν, Young's modulus E, the bulk modulus K, and the shear modulus G. As the density of the sample increases, all the elastic constants increase. Correct to the measurement error, they do not depend on grain size. The results of the crystal measurements coincides with the published data [6]. The density dependence of C_1 and C_2 can be expressed by means of the linear relations

$$C_1 = 3.47\ \rho_{00} - 2.95, \quad C_2 = 1.90\ \rho_{00} - 1.49$$

where C is in km/sec, and ρ in g/cm^3. At $\rho_{00} = 1.87$ g/cm^3, C_1, C_2, and C_3 are equal to 3.54, 2.06, and 2.64 km/sec, respectively. At $\rho_{00} = 1.89$ g/cm^3, $C_1 = 3.61$, $C_2 = 2.10$, and $C_3 = 2.68$ km/sec.

The particle velocity profiles for explosion and impact, respectively, are presented in Fig. 3a and b. At maximum particle velocities less than approximately 850 m/sec, a precursor with a diffuse front is formed ahead of the shock wave. Its entry velocity is about 3.5 km/sec, which coincides with the measured velocity of the longitudinal acoustic waves. Accordingly, the precursor is evidently an elastic wave. Correct to the measurement error, its velocity does not depend on the shock wave intensity. On the interval $300 \leqslant u \leqslant 850$ m/sec, the precursor is followed by a wave with a shock wave front. At $u \leqslant 300$ m/sec, the wave front becomes diffused and at lower values of the maximum particle velocity it can no longer be regarded as a shock front. The development of these characteristics of the shock wave profile in the loading region does not depend on the nature of the source of the shock waves, but is determined only by their intensity. The wave rise time increases with distance traveled and under the experimental conditions approaches 7 μsec. The hodograph of the entry (curve I) and wave maximum (curve II) velocities for impact is plotted in m,t coordinates in Fig. 4. Here, m is the mass coordinate, and t time. The same figure includes the lines of equal particle velocities, obtained from an analysis of the experimental oscillograms. On each of these the value of the particle velocity is given in m/sec. The constant-velocity lines start from the point $m = 0.4$ g/cm^2, where $u \approx 800$ m/sec, at the moment of formation of the two-wave configuration, and end on the line of the wave maximum. The propagation velocity of the maximum decreases at $m \leqslant 1$, but at large distances begins to increase. The inclination of the constant-velocity lines to the m axis decreases as the particle velocity falls.

At low pressures, when the wave front is diffuse, the dynamic compression parameters were determined by integrating the equations of motion and continuity over a given particle velocity field in the loading region (for impact see Fig. 4):

$$\frac{\partial p\,(m,\ t)}{\partial m} + \frac{\partial u\,(m,\ t)}{\partial t} = 0$$
$$\frac{\partial V\,(m,\ t)}{\partial t} = \frac{\partial u\,(m,\ t)}{\partial m} \qquad (2)$$

TABLE 1

u km/sec	N, km/sec	ρ/ρ_0	p, kbar	$E\cdot10^{-6}$, erg/g	$E_x\cdot10^{-6}$, erg/g	ΔT, °C
0.052	1.80	0.893	2.6	0.019	0.003	2
0.085	1.70	0.908	3.7	0.050	0.008	5.2
0.157	1.56	0.947	6.2	0.150	0.023	15.2
0.236	1.70	0.992	8.7	0.304	0.053	30.6
0.282	1.90	1.018	10.2	0.420	0.093	39.2
0.4	2.37	1.047	18	0.8	0.30	61
0.6	3.17	1.073	36	1.8	0.63	143
0.8	3.53	1.125	53.5	3.2	1.16	249
1.0	3.95	1.166	75.4	5.0	1.90	378
1.2	4.34	1.203	98.8	7.2	2.70	548
1.4	4.69	1.241	124.5	9.8	3.60	755
1.6	4.97	1.284	150.7	11.6	4.84	824
1.8	5.24	1.326	176.5	16.2	6.52	1180

where P(m,t) is the normal stress.

Integrating (2), we obtain

$$p(m, t) = -\int_M^m \frac{\partial u(m, t)}{\partial t}\, dm + \varphi(t) \quad V(m, t) = \int_T^t \frac{\partial u(m, t)}{\partial m}\, dt + \psi(m). \tag{3}$$

System (2) is integrated from the elastic wave front with coordinates M, T, at which it was assumed that $p = 0$, $V_1 = V_{00}$. Hence, $\varphi(t) = 0$, $\psi(m) = v_{00}$. Then, integrating the first equation at $t = T$, and the second at $m = M$, by virtue of the condition $u(M,T) = 0$, we obtain

$$p(m, t) = -\frac{\partial}{\partial t}\int_M^m u(m, t)\, dm, \qquad V(m, t) - V_{00} = \frac{\partial}{\partial m}\int_T^t u(m, t)\, dt. \tag{4}$$

Equations (4) were solved numerically in accordance with a difference scheme. Denoting

$$J(m, t) = \int_M^m u(m, t)\, dm, \quad r(m, t) = \int_T^t u(m, t)\, dt$$

we rewrite (4) in the form

$$p(m_i, t_i) = -\frac{J(m_i, t_i + \Delta t_i) - J(m_i, t_i - \Delta t_i)}{2\Delta t_i}$$
$$V(m_i, t_i) - V_{00} = \frac{r(m_i + \Delta m_i, t_i) - r(m_i - \Delta m_i, t_i)}{2\Delta m_i} \tag{5}$$

Equations (5) give the values of the normal stress p and the specific volume V at any point of the loading region, where u(m,t) is given.

In the region of existence of the shock front we determined the strains from the measured displacement of the electromagnetic sensor according to the equation

$$\varepsilon = \frac{V_{00} - V}{V_{00}} = \frac{1}{\Delta x}\int_0^\tau u(M, t)\, dt, \qquad \tau = \frac{\Delta x}{N}$$

where Δx is the distance between the two sensors, and N is the mean wave velocity on the corresponding base.

The value of u for a given ε was taken equal to the mean of the values of u at the end of the record of the first sensor and at the front of the second. The shock compression parameters were determined from the measured values of u, N and u, ε using the equations of conservation at the front. The parameters of the precursor were neglected. At low pressures, when the wave front is diffuse, the dynamic compression parameters were determined from Eqs. (5).

4. The experimental dependence of the wave velocity on the maximum particle velocity is shown in Fig. 1a. The crosses denote the results of experiments in which N was measured on the base between the two sensors for explosive loading. The dots note the results of determining the wave velocity from the measured value of the relative density and particle velocity in accordance with the equation $N = (u\rho/\rho_{00})(\rho/\rho_{00} - 1)$. The circles denote the velocity of the wave maximum or impact obtained by graphic differentiation of the wave maximum hodograph in Fig. 4. The velocity of the maximum is a phase velocity and does not completely characterize the propagation velocity of the compression wave as a whole.

In the region of high shock-wave intensities the experimental data lie on average approximately 3% above the calculated curve 1, which somewhat exceeds the possible systematic error of the experiment. As the particle velocity in the wave decreases, the wave velocity falls sharply, reaching a minimum close to $C_1/2$ at $u \approx 150$ m/sec. With further decrease in u, the velocity of the wave maximum increases, approaching the speed of sound, while theoretical curve 1 tends to zero. The linear N(u) relation $N = 2.68 + 1.43\ u$, drawn through the value of the hydrodynamic speed of sound C_3 at $u = 0$ and the experimental points in the high-pressure region (line 2), describes the experimental results on the interval $u \geqslant 850$ m/sec. At $u = 850$ m/sec it passes approximately 5% above the experimental data.

The relation $u(\rho/\rho_0)$ calculated from Eqs. (1) and the experimental data are presented in Fig. 1b. The notation is the same as in Fig. 1a. In the low-compression region, the material acquires the density of the single crystal at a value of the maximum particle velocity in the wave $u \approx 250$ m/sec. The value of the particle velocity calculated from Eq. (1) for $\rho/\rho_0 = 1$ is equal to zero. At $\rho/\rho_0 > 1.03$ the experimental data conform to the calculated curve 1, but lie slightly above it.

In Fig. 2 the normal stresses calculated from the experimental points NaCl are plotted as a function of ρ/ρ_0. The notation for the experimental points is the same as in Fig. 1a and b. On the range $\rho_0/\rho > 1.03$ the experimental results are in agreement with calculation (1) (curve 1). The observed discrepancy of about 6% corresponds to that of the N(u) relation in Fig. 1a. The same graph shows the low-pressure region to an enlarged scale. The data obtained in the explosion experiments ($\rho_{00} = 1.890$ g/cm^3) for a small wave rise time lie above the data obtained for impact-excited long waves ($\rho_{00} = 1.87$ g/cm^3).

Compression to crystal density occurs at a stress of about 9 kbar. By extrapolating the experimental curve to curve 2, describing Hooke's law for plane strain, we can estimate the value of the dynamic yield stress Y. In the explosion and impact experiments, Y was equal to 1.5 and 0.8 kbar, respectively. This difference cannot be entirely associated with the difference in the densities of the samples, namely, 1.87 and 1.89 g/cm^3, used in these experiments and the inaccuracy of the experimental data. It may be connected with the dependence of the loading curves on the strain rate. Curve 3', constructed from static compression data for NaCl samples of density $\rho_{00} = 1.87$ g/cm^3 in a rigid ring, lies much lower than the dynamic curve. In static deformation the single-crystal density is reached at a stress of 3 kbar and is three times smaller than for dynamic loading. This also serves to confirm the possible dependence of the loading curves on strain rate. For comparison Fig. 2 also includes the isotherm (curve 3) based on Bridgeman's data [7].

The table gives the average values of the dynamic compression parameters and the results of calculating the internal energy and temperature attained in the shock wave. In the low-pressure region, where the wave front is diffuse,

$$\Delta T = \frac{E - E_x}{c} = \frac{1}{c}\left(\int_V^{V_{00}} p\,dV - \int_V^{V_{00}} p_x\,dV\right)$$

where p and p_x are the stresses in dynamic and static compression, respectively, and c is the specific heat under normal conditions.

5. Our investigation of the behavior of porous NaCl under dynamic loading to pressures of 200 kbar indicates the presence of three different regions of state. In the first region ($u > 850$ m/sec), in the first approximation the material may be regarded as a perfect fluid, and the linear N(u) relation constructed from the experimental data may be used to describe the shock Hugoniot. The Hugoniot calculated from the Mie–Gruneisen equation of state and the Hugoniot of a single crystal [5] lie below the dynamic compression data by an amount slightly exceeding the systematic errors of the experiment. Similar results were obtained in experiments on porous metals [7].

In the second region $250 \leqslant u \leqslant 850$ m/sec, a two-wave configuration is formed. This region is regarded at the region of elastoplastic behavior of the material. The first wave is propaged at a velocity coinciding with the longitudinal speed of sound $C_1 = 3.61$ k/sec. Its front is usually diffuse. This wave is evidently associated with the elastic compression of the material as a whole. The particle velocity of the elastic wave in its region of intersection with the front of the following plastic wave ~ 30 m/sec, which corresponds to a stress of about 1.5 kbar, close to the value of the yield stress determined from the $P(\rho/\rho_0)$ diagram in Fig. 2. The plastic wave front is a shock front, its velocity at $u \approx 300$ m/sec is approximately 1.5 times less than that determined by the linear N(u) relation. In the third region ($u < 250$ m/sec), $\rho \leqslant \rho_0$ (the wave intensity is insufficient to collapse the pores) the plastic wave front is diffused the more strongly, the lower its intensity and the greater the path traveled through the material. The elastic wave joins smoothly with the plastic eave, and it is difficult to distinguish the boundary. The velocity of the wave maximum has a minimum value at $u \approx 150$ m/sec equal to approximately $C_1/2$. At lower values of the particle velocity, the velocity of the wave maximum increases, tending to C_1, since the state of the material then approaches the state of elastic compression. The curve $p(\rho/\rho_0)$ is convex toward the ρ/ρ_0 axis (Fig. 2) in accordance with the nature of the diffusion of the profile in this range of intensities.

There is still no reliable description of the behavior of a porous material dynamically compressed to a density less than the density of the single crystal. Therefore, the results of the dynamic measurements were compared with data on static deformation. There is a sharp difference between the dynamic and static compression curves in the region of stresses in which the material retains its porosity. In these processes the collapse of the pores takes place at 9 and 3 kbar, respectively. The shock compression curve calculated in the usual way from the static curve practically coincides with the latter. The material is not heated. Therefore, the high temperatures calculated from the measured dynamic curve (Table 1) are apparently associated with heating due to friction connected with the crushing of the grains and their plastic flow into the pores. In this case one may expect the loading time to have in influence on the deformation process. Clearly, this also affects the difference between the $P(\rho/\rho_0)$ curves for dynamic loading by short and long waves and the static deformation curve.

The authors thank A. A. Ignatov for his help with the work, L. D. Livshits for the data from the static experiments, and G. P. Demidyuk for providing the opportunity of working with the ultrasonic installation.

LITERATURE CITED

1. I. V. Belinskii and B. D. Khristoforov, "Viscosity of NaCl in shock compression," PMTF, No. 1, 1968.
2. I. V. Belinskii and B. D. Khristoforov, "Attenuation of impact-induced plane shock waves in aluminum," PMTF, No. 3, 1967.
3. Ya. B. Zel'dovich and Yu. P. Raizer, Physics of Shock Waves and High-Temperature Hydrodynamic Phenomena [in Russian], Nuaka, Moscow, 1966.
4. B. Alder, "Physical experiments with strong shocks," in: Solids under High Pressure [Russian translation], Mir, Moscow, 1966.
5. L. V. Al'tshuler, L. V. Kuleshova, and M. N. Pavlovskii, "Dynamic compressibility equation of state and electrical conductivity of sodium chloride at high pressures," ZhETF, 39, 1 (7), 1960.
6. Physical Acoustics [in Russian], Mir, Moscow, 1968.
7. P. W. Bridgeman, "The compression of 46 substances to 50000 kg/cm^2," Proc. Amer. Acad. Arts Sci., 74, No. 3, 1940.
8. I. Thouvenin "Effect of a shock wave on a porous solid," Proc. 4-th Sympos. (Internat.) Detonat. White Oak, Md., 1965, Washington, pp. 258-265, 1967.
9. F. A. Baum, K. P. Stanyukovich, and B. I. Shekhter, Physics of Explosion [in Russian], Fizmatgiz, Moscow, 1959.